Theoretical Investigation on the Effect of Protonation on the Absorption and Emission Spectra of Two Amine-Group-Bearing, Red "Push−Pull" Emitters, 4-Dimethylamino-4′-nitrostilbene and 4-(dicyanomethylene)-2-methyl-6-*p*-(dimethylamino) styryl-4H-pyran, by DFT and TDDFT Calculations

I. D. Petsalakis,[†] D. G Georgiadou,[‡,§] M. Vasilopoulou,[‡] G. Pistolis,[‡] D. Dimotikali,[§] P. Argitis,[‡] and G. Theodorakopoulos*,[†]

Theoretical and Physical Chemistry Institute, The National Hellenic Research Foundation, 48 Vassileos Constantinou Avenue, 116 35 Athens, Greece, Institute of Microelectronics and Institute of Physical Chemistry, NCSR Demokritos, 153 10 Aghia Paraskevi, Greece, and Department of Chemical Engineering, National Technical University of Athens, 15780 Athens, Greece

Received: January 13, 2010; Revised Manuscript Received: March 27, 2010

A theoretical investigation on the electronic structure of 4-dimethylamino-4′-nitrostilbene (DANS), 4-(dicyanomethylene)-2-methyl-6-p-(dimethylamino) styryl-4H-pyran (DCM), and their protonated forms is presented in an effort to rationalize recent experimental results on the tuning of the emitted color of organic light-emitting diodes through photochemically induced protonation. Density functional theory (DFT) and time-dependent density functional theory (TDDFT) calculations have been carried out on the neutral and protonated forms of DANS and DCM, employing both the B3LYP and the CAM-B3LYP functionals. It was found that the CAM-B3LYP functional leads to better agreement than the B3LYP of the calculated with the experimental absorption λ_{max} for DANS, whereas B3LYP is more appropriate than CAM-B3LYP for DCM. The results of the calculations aid in a rationalization of the observed differences of the spectra of DANS and DCM upon protonation, and in particular those differences that make DANS a more attractive system for absorbance and emission tuning.

Introduction

The molecular compounds 4-dimethylamino-4′-nitrostilbene (DANS) and 4-(dicyanomethylene)-2-methyl-6-p-(dimethylamino)styryl-4H-pyran (DCM) are characteristic examples of the so-called "push−pull" chromophors, where an electron-donor moiety D is coupled to an electron-acceptor moiety A through a π-conjugated bridge. Push−pull chromophors have attracted a great deal of research interest over the years because they are used in nonlinear optics (NLO) applications besides serving as models for intramolecular charge-transfer processes.[1]

The ground and excited electronic states of such chromophors are generally described as linear combinations of neutral and zwitterionic diabatic basis states (D-A) and (D^+-A^-), respectively, with the ground state being predominantly neutral and the excited state predominantly charge-transfer in character.[2] Furthermore, as it has been shown for the (much smaller) 4-(dimethylamino) benzonitrile (DMABN) molecule, a $\pi-\pi^*$ or locally excited (LE) state must be also considered.[3] The LE state is the state from which fluorescence is observed in the gas phase of DMABN, whereas in polar solvents emission from a charge transfer state is also observed. By analogy, it is expected that in the larger compounds, as well, the relative energy of their excited states will depend on the polarity of the solvent as well as on the molecular geometry, with a twisted internal charge transfer structure possibly characterizing the first excited state in polar solvents. To this effect there have been many experimental and theoretical investigations on the photophysics of both DANS and DCM in different solvents[2,4–14] in order to examine the evolution of the absorbing state, and in particular the degree of intramolecular charge separation in the emitting state, which is manifested by the large Stokes shift in polar solvents.

In the last two decades certain push−pull chromophors have also been used extensively as fluorescent emitters of organic light emitting diodes (OLEDs) for display and solid state lighting applications.[15] Colored emission in electroluminescent devices is obtained, usually, by doping fluorescent or phosphorescent compounds into host materials with a larger band gap. In this context DCM in particular is a very well-known red emitter for OLEDs, introduced in one of the first publications in this field by Tang and Van Slyke in 1989.[16]

Recently, the chromophors DANS and DCM have been evaluated as red emitters dispersed in polymer films in investigations of color tuning in OLEDs.[17] In that work it was demonstrated that it is possible via illumination in the presence of a photoacid generator to either allow (when the red emitter is in its neutral form) or suppress (when the red emitter is in its protonated form) red frequencies. Furthermore, in the case of DANS, it was shown that a sizable blue shift of the absorbance is obtained upon protonation, and this finding was implemented to achieve photoguided definition of red, green, and blue emitting areas in a single emissive layer containing this emitter along with an acid-sensitive green emitter (DMA-DPH), as has been described in detail in the relevant reports.[17,18]

In the present work, a theoretical investigation is carried out on the electronic structure of DANS and DCM as well as the corresponding protonated forms in an effort to rationalize the experimental observations by correlating differences in their

* To whom correspondence should be addressed.
[†] The National Hellenic Research Foundation.
[‡] Institute of Microelectronics and Institute of Physical Chemistry.
[§] National Technical University of Athens.

10.1021/jp100338d
Published on Web 04/12/2010

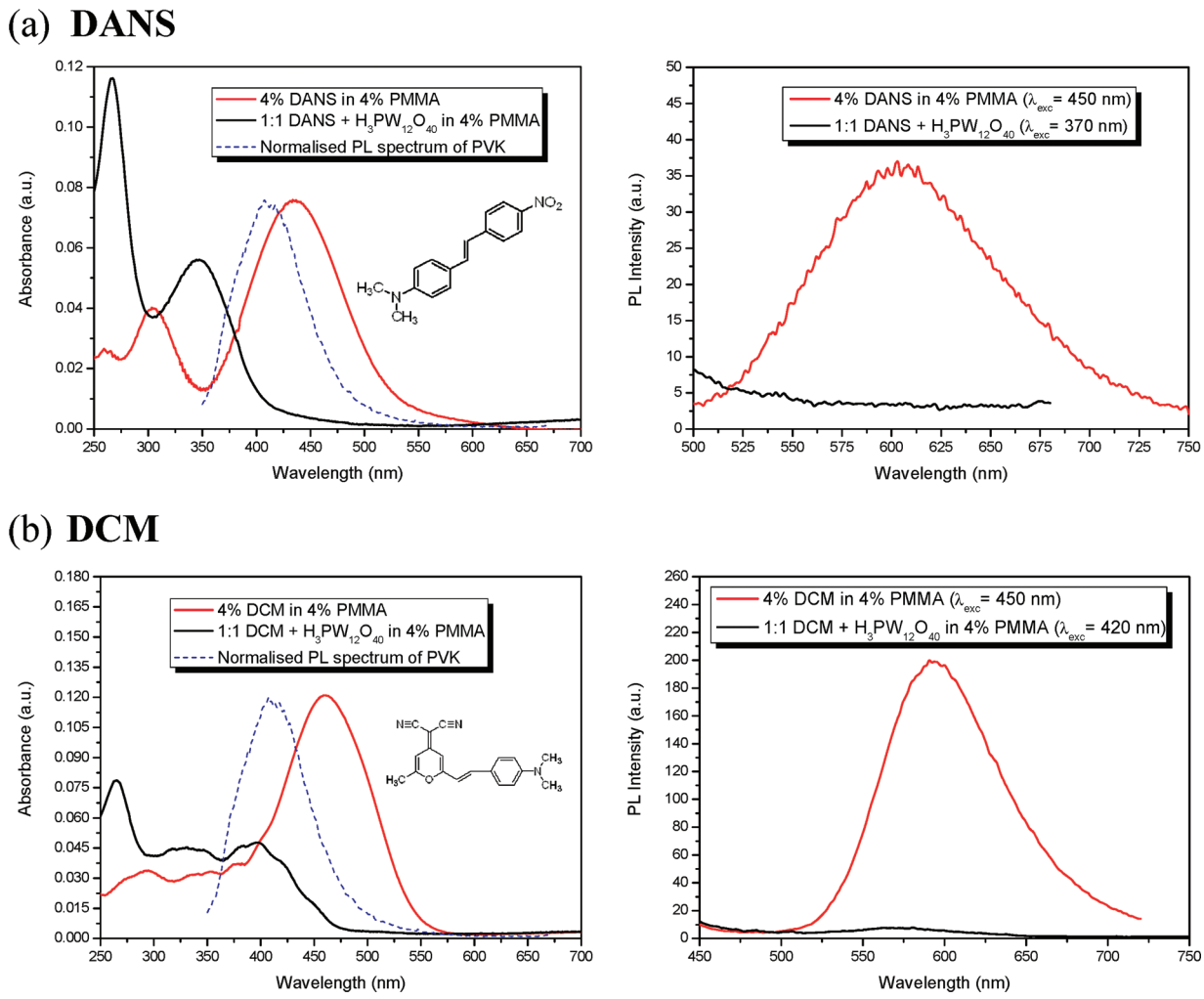

Figure 1. Absorption (left) and fluorescence (right) spectra of (a) DANS and (b) DCM in a PMMA matrix before and after protonation by the strong Brønsted acid $H_3PW_{12}O_{40}$ (dodecatungstophosphoric acid). The spectrum of PVK emission is also plotted in order to demonstrate the successful energy transfer to unprotonated DANS and its subsequent suppression upon protonation of the dye. The PVK spectrum is scaled to the absorption spectra. The structures of DANS and DCM can also be seen.

electronic structure with their observed differences in performance as absorbers or emitters. In this manner, the present theoretical investigation might assist in the quest for emitters suitable for the design of OLEDs with desirable emission characteristics[19] or for exploitation in sensing applications.[20]

The theoretical results are compared with experimental data from the literature. In the case of DANS, which is more interesting for the current work due to its clear and sizable absorbance blue shift, experimental absorption and fluorescence spectra in different solvents were also obtained for both the neutral and protonated forms, to complement the literature data.

Calculations

The molecular compounds of interest (their structures can be seen in Figure 1) involve a large number of atoms and the most appropriate methods for electronic structure calculations are density functional theory[21] (DFT) and time-dependent DFT[22] (TDDFT) for the excited states. Ab initio configuration interaction (CI) calculations would be impossible for the present systems, whereas with the RICC2 method,[23] which is considered to be a good alternative for medium-size systems, there exists the problem of inclusion of the solvent. Although there are well-known problems often found with DFT/TDDFT for calculations on charge transfer states[24] leading to underestimation of the relevant excitation energies, useful information can be obtained and it is possible to draw qualitative information even from the electron-density plots of the frontier orbitals involved in the excitations.[25] Furthermore, making use of functionals specifically developed to have the correct asymptotic behavior is expected to aid in the calculation of charge-transfer states.

In the present work, DFT and TDDFT calculations have been carried out on DANS, DCM, and their protonated forms at a first stage using the B3LYP[26] functional and triple-zeta (TZVP and DGTZVP[27]) basis set. Subsequently, with the release of Gaussian 09,[28] it became possible to employ the CAM-B3LYP functional[29] as well for the calculations, and this was done along with the 631G(d,p) basis set, for the isolated molecules and also for the molecules in different solvents. The CAM-B3LYP functional has been reported to correct for long-range interactions and to perform better than B3LYP for the calculation of charge-separated states.[29]

The different solvents have been included with the aid of the polarized continuum model (PCM)[30] offered as default in Gaussian 09. This model is considered to be the most successful for accounting for the solvent effects in DFT and TD-DFT calculations. For example, extensions of the model by the inclusion of solvent molecules explicitly have been described very recently,[31] involving a locally modified version of Gaussian.

They found only small red shifts (e.g., from 466.8 to 480.2 nm in absorption, with the experimental λ_{max} at 547.0 nm of tetramethylrhodamine isocyanate[31]) between the PCM model and the extended model.

With both the B3LYP and the CAM-B3LYP functionals, excited electronic states have been calculated at the optimized ground state geometry, relevant to the absorption spectra of the systems of interest. Subsequently, calculations involving geometry optimization of the first excited state are carried out, yielding information relevant to the emission spectra. All the initial stage calculations on the optimization of the excited state geometries in the absence of any solvent were carried out with the aid of TURBOMOLE and employing the B3LYP functional. At the second stage, geometry optimization calculations for the excited states, with and without solvent and the CAM-B3LYP as well as B3LYP functionals, were carried out with the aid of Gaussian 09, which offers the facility of including the solvent for the excited state geometry optimization as well as the use of the CAM-B3LYP functional. The starting geometry for all the geometry-optimization calculations on the excited states was the absorption geometry, that is, the ground-state optimum geometry, unless otherwise stated.

The geometry optimization calculations on the excited states are not always successful, especially for interacting states and also if a solvent is included. The objective of primary importance here is to determine the differences in the excited states of the protonated versus the neutral forms of DANS and of DCM and to relate these differences to the observed differences in the absorption spectra of the two systems dispersed in polymer films.

The programs Gaussian 03, Gaussian 09,[28] and TURBOMOLE[32] have been employed for the calculations. Electron-density plots have been constructed using GaussView 5.[28]

Results and Discussion

The two push−pull chromophors studied in the present work both bear a dimethylamino group as the electron donor moiety. This amine group is prone to protonation in the presence of acid, resulting in changes of the absorbing and emitting properties. Protonation can be induced either by the addition of a Brønsted acid (e.g., dodecatungstophosphoric acid, $H_3PW_{12}O_{40}$) in solution or in solid state, or photochemically in the presence of a photoacid generator (PAG). Photoacid generators are compounds such as sulfonium salts, which release a proton upon illumination at a certain wavelength via a photochemical reaction.[17]

During operation of OLEDs based on doped systems, dopants can be excited through energy transfer from the host.[16] According to resonance energy transfer theory,[33] an efficient Förster energy transfer requires, among others, a large overlap between host (polymer) emission and acceptor (dopant) absorption.

As previously reported,[17] the efficient energy transfer, occurring from the wide band gap conducting polymer PVK to the DANS dopant due to the sufficient overlap of their emission and absorption spectra, respectively, is disrupted when the DANS emitter is protonated by the strong Brønsted acid $H_3PW_{12}O_{40}$. In this case, the absorption spectrum of protonated DANS no longer overlaps with the emission spectrum of PVK, allowing the observance of PVK blue emission or the emission of other dopants.[17,18] Conversely, the well-known and commonly used DCM emitter does not perform well in this aspect, as the absorption of the protonated form does not show a distinct blue shift and continues to absorb basically in the same region as the initial DCM, resulting in quenching of the host polymer emission.[17]

Absorption and photoluminescence spectra of DANS, DCM, and their protonated forms in poly(methyl methacrylate) (PMMA) matrix are presented in Figure 1, where PMMA was chosen as more appropriate for illustration purposes, since it is transparent at wavelengths above 250 nm and the absorption shift of the dyes upon protonation can be better monitored (the dyes studied here absorb at wavelengths greater than 300 nm). Furthermore, PMMA is a well-known nonreactive and thermally stable polymer (in the conditions of the experiments). As can be seen in Figure 1, the initial absorption band of DANS at 445 nm disappears after protonation, and a new band appears at 340 nm, corresponding to the protonated form. In the case of DCM, the initial absorption band has a maximum at 460 nm, whereas the protonated form does not show a distinct maximum in the region 250−650 nm of the spectrum. On the other hand, for both DANS and DCM the initial fluorescence (maximum at 620 and 610 nm, respectively) practically disappears after protonation.

In addition to the absorption and photoluminescence spectra of DANS, DCM, and their protonated forms in PMMA, we have proceeded to record the spectra of DANS and protonated DANS in solvents of differing polarity. The relevant data have been used to complement literature data and they are presented in Table 1 for a direct comparison with the results obtained by the theoretical calculations.

A. Results of the Calculations on DANS. The results of the B3LYP and CAM-B3LYP calculations on DANS (and protonated DANS) are summarized in Table 1 in terms of the lowest energy absorption and emission maxima calculated for the isolated systems as well as in different solvents, along with experimental data, where available. In Figure 2, the optimum geometries of the ground and first excited state (S_1) of isolated DANS and protonated DANS, as well as electron density plots of the frontier orbitals in the different structures, are given. It can be seen that the optimum geometry of the ground electronic state of DANS is a planar structure with the two phenyl rings, with the bridging double bond and the -NO_2 moiety in the same plane (see structure I in Figure 2), as obtained by both the B3LYP and CAM-B3LYP geometry optimization. The optimum geometry of the lowest excited state as calculated by B3LYP geometry optimization is a twisted structure, where the acceptor group (-phenyl-NO_2) lies at a plane vertical to the plane of the remaining molecule (see structure II-twisted in Figure 2). Conversely, the optimum structure of S_1 determined by the CAM-B3LYP calculation is a planar structure (structure II-planar in Figure 2) similar to that of the ground state. The question of the optimum geometry of the S_1 state of DANS was further investigated by CAM-B3LYP with starting point the twisted S_1 minimum of the B3LYP calculation. This procedure resulted in a minimum energy twisted structure, at higher energy than the planar only by 0.06 eV, with vanishing oscillator strength with the ground state. In this manner, we have identified a planar as well as a twisted minimum energy structure for the S_1 state of DANS in the isolated system.

As shown in Table 1 and will be discussed further below, generally higher transition energies (smaller λ_{max}) are obtained with the CAM-B3LYP functional than with B3LYP, for both absorption and emission. At the ground state geometry, the lowest excited state, S_1, calculated with the B3LYP functional corresponds to absorption at 467 nm with large oscillator strength (see Table 1), which is in good agreement with the 445 nm experimental absorption maximum of DANS in PMMA matrix discussed in the previous section. This state is described mainly as an electron excitation HOMO → LUMO, which, as the electron density plots show, involves transfer of electronic

TABLE 1: Results of DFT and TDDFT Calculations on the S_1 State of DANS in the Initial and Protonated Forms, in Different Solvents[a]

	λ_{max}(nm), f-value					
	DANS			Protonated DANS		
transition:[b] solvent	B3LYP	CAM-B3LYP	exp[c,d,e,f]	B3LYP	CAM-B3LYP	exp
A: $S_0 \rightarrow S_1$	467, 0.77	352, 1.22	336[c]	353, 1.09 (S_1)	315, 0.002 (S_1)	
no solvent				347, 0.0008 (S_2)	306, 1.19 (S_2)	
A: toluene	557, 0.75	390, 1.38	*428*		322, 1.37	*357*
A: THF	609, 0.84	432, 1.31	*432*, 426[d]	377, 1.22	329, 1.44	*338*
A: chloroform		397, 1.44	*437*, 434[d]		325, 1.43	*334*
A: acetone	535, 0.91	412, 1.49	*430*, 433[d]	385, 1.09	335, 1.45	
A: acetonitrile	557,1.01	412, 1.50	435[d]	391, 1.19	336, 1.45	
E: $S_1 \rightarrow S_0$						
no solvent	680, 0.00	401, 1.39	369[c]	780,0.00 (S_1)	625, 0.00 (S_1)	
	334, 0.29 (S_3)			379, 0.72 (S_3)	321, 1.33 (S_2)	
E: toluene		459, 1.59	*556*, 583[d]		395, 1.41	
E: THF		501, 1.74	*637*, 670[d], 683[e]	451, 1.41	414, 1.52	
E: chloroform		485, 1.69	*680*, 735[d], 725[e]		406, 1.50	*592*
E: acetone		523, 1.79	*706*, 800[e], 767[e]		426, 1.55	
E: acetonitrile	632, 1.10	529, 1.81	>850[d]	464, 1.81	429, 1.55	

[a] Experimental λ_{max} in different solvents of the present work in italics. Experimental λ_{max} in PMMA matrix in footnote. [b] A: absorption (ground state optimum geometry), E: emission (excited state S_1 optimum geometry). [c] Reference 1a. [d] Reference 5b. [e] Reference 10. [f] Experimental data in PMMA matrix, see text: DANS A: 445 nm, E: 620 nm, protonated-DCM A: 340 nm.

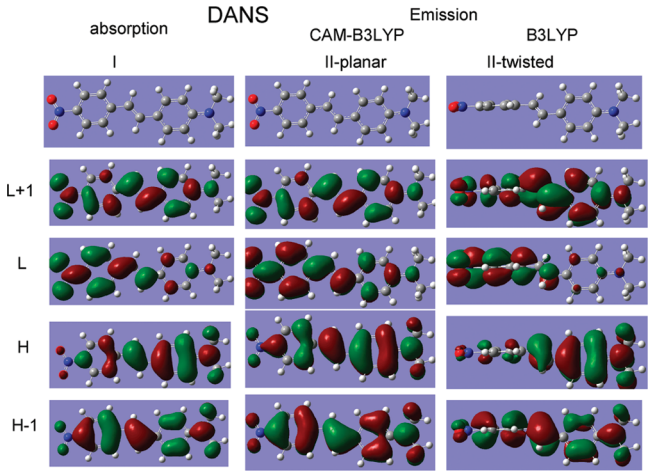

Figure 2. Equilibrium structures for the ground and lowest singlet excited state of DANS (structures I, II-planar, and II-twisted) and electron density plots of the frontier molecular orbitals; H stands for highest occupied and L for lowest unoccupied orbitals.

charge from the amine part (donor) to the nitro part (acceptor) of the molecule (see Figure 2). At the twisted structure, II-twisted, the dominant excitation characterizing S_1 is still HOMO → LUMO, but in this case the HOMO and LUMO show totally separated charge densities; see Figure 2. At the twisted (B3LYP-optimum) S_1 geometry, a very low *f*-value is calculated for a transition from the ground state to S_1, at 680 nm, again in good agreement with the observed fluorescence maximum of DANS in a PMMA matrix (Figure 1a). However, the apparent agreement of the B3LYP values with the experimental absorption and emission maxima in a PMMA matrix results from a cancellation of the errors inherent in the B3LYP functional for the excitation energies of charge-transfer states with those due to the lack of inclusion of the effect of the solvent-matrix. As shown in Table 1, for the entries with no solvent, the B3LYP absorption energy is about 1 eV smaller than the vapor-phase experimental[1a] λ_{max}, whereas the CAM-B3LYP value is larger than the experimental by only 0.14 eV. Therefore, we have here an example where the CAM-B3LYP functional lead to a more accurate determination of the energy difference between the ground and an excited charge-transfer electronic state. Similarly, for emission in the absence of solvent (see Table 1), it may be noted that again the CAM-B3LYP result at 401 nm (with the B3LYP value at 680 nm) is in good agreement with the observed emission at 369 nm.[1a] As noted above, the B3LYP calculations lead to a twisted equilibrium structure for S_1 with vanishing oscillator strength, and similarly for the second excited singlet electronic state, S_2, and only the third excited state, S_3, at 334 nm is found to have significant oscillator strength with the ground state, at the twisted geometry minimum of S_1.

As already mentioned, the effect of different solvents on the absorption and emission maxima have been the subject of intense experimental work,[5] and similarly, there exist a number of previous calculations, mostly semiempirical but also ab initio, on the vertical spectrum of DANS at the ground state equilibrium geometry, including as well the effect of different solvents.[2,4] In the present work, we have carried out TD-DFT calculations including the geometry optimization of the S_1 state in the presence of solvents of different polarity. Our results, included in Table 1, show that, as was the case in the absence of solvent, the absorption maxima in different solvents are calculated more accurately with the CAM-B3LYP functional, and they are in good agreement with the available experimental data.

Optimization of the geometry of the first excited singlet state of DANS in the presence of different solvents was successfully carried out with the CAM-B3LYP functional, whereas with the B3LYP the calculations did not converge, and only for the cases of acetonitrile solvent did the geometry optimization converge, yielding a planar structure for the S_1 state. As shown in Table 1, the agreement between the calculated (CAM-B3LYP) and experimental emission maxima is not as good as for absorption maxima, with discrepancies between the experimental and theoretical values ranging from 0.51 eV (toluene) to 0.97 eV (acetone), where the theoretical transition energies are larger than the experimental. These large discrepancies may indicate that the geometry optimization of the excited state in the presence of solvent is not as successful as without the solvent. The alternative explanation might be the existence of a nonplanar geometry energy minimum for the excited state, such as calculated for example for the vapor phase system, at which

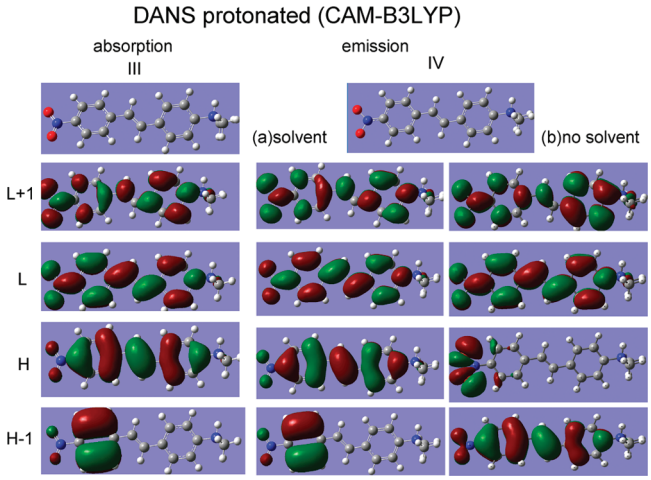

Figure 3. Equilibrium structures for the ground and lowest singlet excited state of protonated DANS (structures III and IV) and electron density plots of the frontier molecular orbitals, H stands for highest occupied and L for lowest unoccupied orbitals. (a) Frontier orbitals at geometry IV in the presence of solvent; (b) frontier orbitals at IV in the absence of solvent.

the emission maximum might be at smaller energies (longer wavelengths) in solvents. Nevertheless, it was not possible for the geometry optimization calculations to converge in the presence of a solvent at any nonplanar structures, with either the B3LYP or the CAM-B3LYP functionals.

Protonation of DANS at the amine nitrogen atom is calculated to be very favorable, leading to an energy lowering with respect to the neutral by 9.8 eV. Geometry optimization yields similar geometries for the ground and the first excited state of protonated DANS (see Figure 3, structures III and IV respectively), that is, nearly planar (III, 5.5° dihedral angle of the -phenyl-NO_2 moiety) and planar (IV) structures with only the two methyl groups placed above and below the plane of the rest of the molecule. The results on the optimum geometries (III and IV) are similar, whether or not a solvent is included in the calculation. Similarly, the electron density plots of the frontier orbitals at the absorption geometry III (i.e., the optimum geometry of the ground electronic state) remain the same in the presence of solvent as in the isolated protonated DANS and also for IV in the presence of a solvent (see (a) under IV in Figure 3). However, in the absence of any solvent, at geometry IV, it turns out that the electron density distribution of HOMO−1 is that of HOMO in III and IV(a), and HOMO at IV(b) is as HOMO−2 in III and IV(a).

The CAM-B3LYP calculations on protonated DANS at the ground state equilibrium geometry, in the absence of any solvent, find the second excited state as the absorbing state, characterized by a HOMO → LUMO excitation at 306 nm and *f*-value of 1.19, with the lowest excited singlet state calculated at 315 nm with 0.0018 oscillator strength (see Table 1) and characterized mainly by an excitation from HOMO−2 (not shown in Figure 3, but with electron density localized at the -NO_2 moiety). Inclusion of different solvents in the calculation of protonated DANS yields the lowest excited state S_1 (HOMO → LUMO) as the absorbing state in both the B3LYP and the CAM-B3LYP calculations. The calculated absorption maxima are only moderately shifted to the red with respect to λ_{max} in the isolated protonated DANS system. Again, the CAM-B3LYP results are closer to the experimental maxima, but the B3LYP are not as far off as in the unprotonated system. The experimentally interesting feature of a blue-shifted absorption maximum of the protonated DANS with respect to neutral DANS in a PMMA matrix is also observed to varying degrees in different solvents (see experimental values in Table 1). The experimental shift in toluene is by 71 nm, in THF by 94 nm, and in chloroform by 103 nm. The corresponding theoretical shifts (focusing on the CAM-B3LYP results) are 46 nm in the absence of solvent, 68 nm in toluene, 77 nm in acetone, 103 nm in THF, and 72 nm in chloroform.

At the optimum geometry of S_1 of protonated DANS, in the absence of any solvent, the lowest singlet excited state calculated with the CAM-B3LYP functional (lowest two excited states with B3LYP), S_1, is characterized by the HOMO → LUMO excitation and has negligible transition probability to the ground state and only the second excited state S_2 (HOMO−1 → LUMO) at 321 nm (S_3 at 379 nm, B3LYP) is predicted to have appreciable emission (see Table 1). Taking into account the fact the changes in the electron density distributions of HOMO and HOMO−1 between geometries III and IV(b), it is obvious that the same excited state of protonated DANS that is predicted to have significant absorption probability is also found to have significant emission probability and is calculated as the second excited state, or S_2, in the absence of any solvent, whereas the lowest excited state S_1 is characterized by an excitation involving transfer of electron density from the -NO_2 moiety to the rest of the molecule. In the presence of solvents, all the calculations find that the S_1 (HOMO → LUMO) state of protonated DANS at its optimum geometry has appreciable oscillator strength (see Table 1). Thus, the S_1 state calculated in the presence of solvents is the S_2 state (focusing only on the CAM-B3LYP calculations) calculated in the isolated protonated DANS. Further geometry optimization calculations have been carried out for isolated protonated DANS, this time on the S_2 state, with starting point the geometry of S_1 and also the absorption geometry. Both optimizations resulted in identical optimum geometry for S_2, and it is found to be similar to that of the ground state and of S_1, (see structures III and IV of figure 3). Furthermore, at the optimum geometry of S_2 the electron-density distribution of the frontier orbitals is as in III and IV(a) and S_2 is in fact the lowest state, characterized by the HOMO → LUMO excitation and calculated at 364 nm with oscillator strength 1.22 while the state characterized by the charge-transfer excitation is now calculated at 328 nm, that is, as the second excited state. Therefore, between the S_1 minimum at 625 nm and the S_2 minimum at 364 nm (labeling the states at their relative position at absorption) there exists an avoided crossing between the potential energy surfaces of the first and second excited states, and the S_2 minimum is in fact a local minimum on the lowest excited state potential, lying 0.66 eV higher than the S_1 minimum.

Emission from protonated DANS was not observed in the different solvents, except for the case of chloroform, where the theoretical emission maximum yields transition energy higher than the experimental by about 1 eV, and it is shifted to the blue by 79 nm (with respect to neutral DANS in chloroform) with experimental shift by 88 nm.

It is interesting to note that the calculations on the absorption spectrum of DANS in different solvents and protonated DANS in different solvents yield the same pattern, that is, the lowest singlet state S_1 absorbing with high oscillator strength and the higher excited states S_2 to S_5 have either vanishing or very low oscillator strength. This is in accord with the existence of the distinct absorption maximum in DANS and (blue-shifted) in protonated DANS in the experimental spectra.

TABLE 2: Results of DFT and TDDFT Calculations on the S_1 State of DCM in the Initial and Protonated Forms, in Different Solvents[a]

	λ_{max}(nm), f-value				
	DCM			Protonated DCM	
transition:[b] solvent	B3LYP	CAM-B3LYP	exp.[c,d,e]	B3LYP	CAM-B3LYP
A: $S_0 \rightarrow S_1$No solvent	436, 1.11	371, 1.32		568, 0.18	399, 0.36
A: toluene	469, 1.30	398, 1.51		467, 0.33	364, 0.72
A: DMSO	495, 1.38	423, 1.64	476[d], 480[e]	416, 0.71	361, 1.16
A: chloroform		412, 158			360, 0.95
A: acetone		426, 1.64			361, 1.13
A: acetonitrile	497, 1.41	427, 1.65	460[e]	416, 0.69	361, 1.16
A: ethanol	493, 1.38	422, 1.63	472[d]	418, 0.67	361, 1.14
E: $S_1 \rightarrow S_0$ No solvent	571, 0.41	437, 1.23		737, 0.13	534, 0.30
E: toluene		468, 1.58			479, 0.61
E: DMSO	547, 1.64	521, 1.79	635[d], 634[e]	559, 0.57	456, 1.14
E: chloroform		491, 1.68			462, 0.85
E: acetone		516, 1.77			456, 1.10
E: acetonitrile	546, 1.63	520, 1.78	615[e]	560, 0.56	456, 1.13
E: ethanol	544, 1.63	518, 1.78	615[d]	563, 0.54	456, 1.11

[a] Experimental λ_{max} in PMMA matrix in footnote. [b] A: absorption (ground state optimum geometry), E: emission (excited state S_1 optimum geometry). [c] Experimental data in PMMA matrix, see text: DCM A: 460 nm, E: 610 nm; protonated DCM A: <450 nm. [d] From ref. 7. [e] From ref 13.

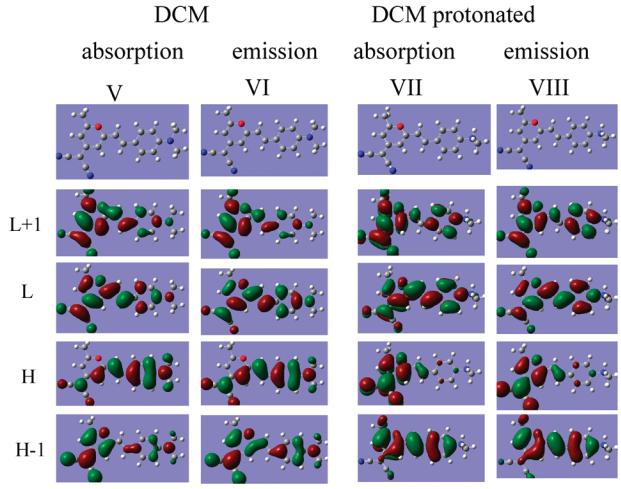

Figure 4. Equilibrium structures for the ground and lowest singlet excited state of DCM (structures V and VI) and protonated DCM (structures VII and VIII) and electron density plots of the frontier molecular orbitals; H stands for highest occupied and L for lowest unoccupied orbitals.

B. Results of the Calculations on DCM. The results of the calculations on DCM are summarized in Table 2 and Figure 4. The geometry optimization calculations of DCM obtain a planar structure for both the ground and the first excited electronic states (structures V and VI, Figure 4) in the isolated molecule as well as in the presence of the solvents, and the electron density plots of the MO at these two geometries are similar. The same results on the geometries are obtained with both the B3LYP and the CAM-B3LYP functionals and Figure 4 has been constructed using the results of the CAM-B3LYP calculations. In the isolated molecule, at both the ground state (structure V) and the S_1 equilibrium geometry (structure VI), the lowest excited state (HOMO → LUMO excitation) involves a transfer of electronic charge from the amine toward the pyran moiety of the molecule (see Figure 4).

The time evolution of the S_1 state of DCM has been studied experimentally,[6,13] investigating the evolution from an LE state to a possible twisted-geometry charge-transfer state. This evolution has been found to depend very much on the solvent and to most likely involve torsion of the dimethyl-amino group.[13] A theoretical study of intramolecular charge transfer in DCM suggests ICT states twisted either at the dimethylanilino group or at the dimethylamino group, which gain importance in the emission spectra in polar solvents.[8] In the present work, optimization of the geometry of the S_1 state in the presence of different solvents always leads to a planar equilibrium geometry for DCM in the S_1 state.

The absorption and emission maxima calculated for DCM isolated and in different solvents are collected in Table 2, along with those of the calculations on protonated DCM (to be discussed below). In all cases, the B3LYP absorption maxima are red-shifted by 60−70 nm with respect to the CAM-B3LYP and are in good agreement with the available experimental data. Again, most geometry optimizations on S_1 were obtained using the CAM-B3LYP functional, and the calculated emission maxima are generally at higher energies than the experimental. Except for the case of no solvent, the B3LYP values for the emission maxima, where available, are very close to the CAM-B3LYP.

Protonation at the amine nitrogen atom of DCM is calculated (as in DANS above) to be very favorable, again leading to an energy lowering with respect to the neutral of 9.7 eV. As shown in Figure 4, geometry optimization for the ground (see structure VII) as well as for the lowest excited electronic state (structure VIII) yields similar nearly planar structures. The equilibrium geometry for the ground state has a 9.4° dihedral angle between the planes of the two rings, while in the equilibrium geometry of S_1 the corresponding dihedral angle is 27.0°. At the protonated nitrogen, the two N−C bonds are above and below and N−H is coplanar with the plane of the phenyl ring, in both the ground and the excited state equilibrium geometries. Finally, nearly identical electron density plots of the frontier orbitals are found in the ground and in the S_1 equilibrium geometries, but they are different from those calculated for unprotonated DCM (under V and VI in Figure 4). For protonated DCM the lowest excited state involves a transfer of electronic charge from the pyran ring toward the rest of the molecule. Comparing the calculated absorption maxima of DCM with those of protonated DCM, focusing only on the CAM-B3LYP values (see Table 2), it can be seen that in the absence of solvent the absorption maximum of protonated DCM is found at small red shift rather than a blue shift with respect to DCM. Inclusion of different solvents

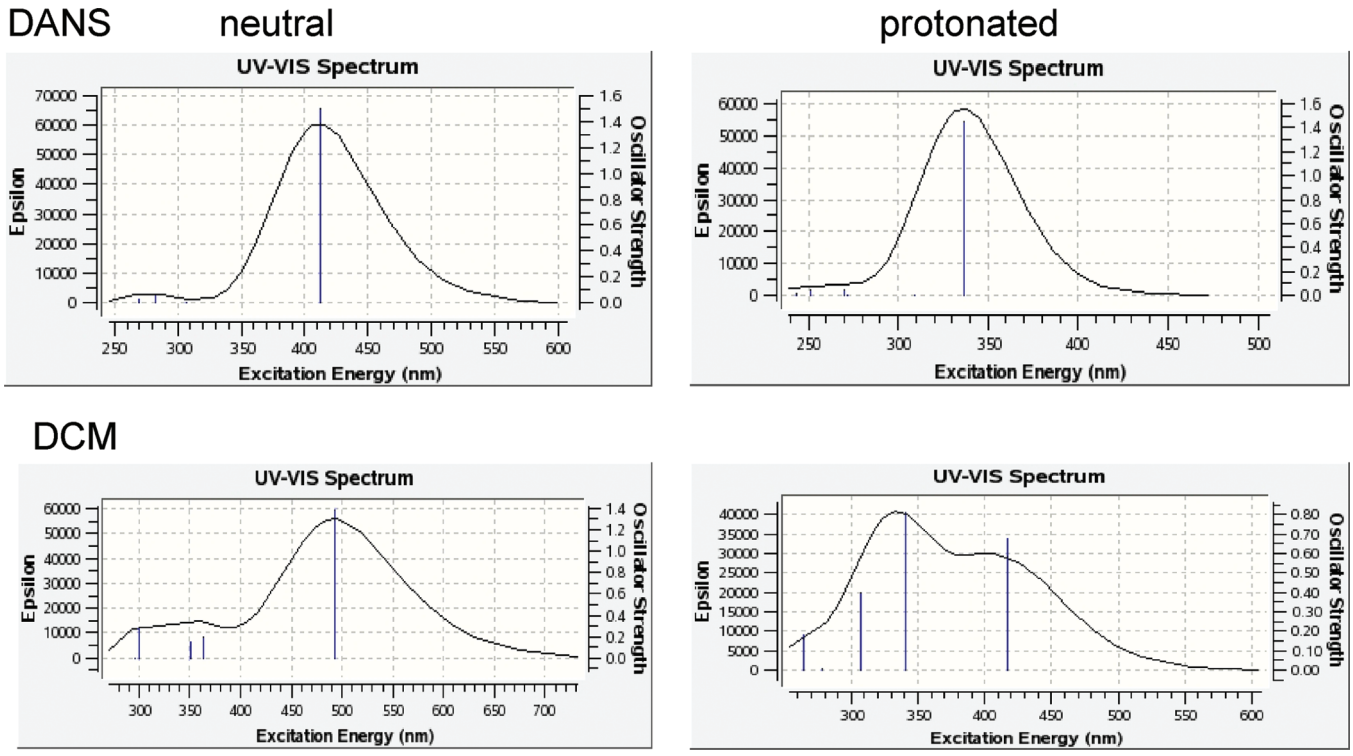

Figure 5. A drawing of the UV−vis spectra of DANS, DCM, and their protonated forms, based on the calculated transition energies and oscillator strengths of the lowest five excited singlet states. For clarity, different horizontal and vertical scales are used in the different plots.

leads to small blue shifts in the absorption maxima calculated for protonated DCM but smaller shifts than in the case of DANS (the largest calculated at 65 nm in acetone). Similarly, in most solvents considered, the emission maximum of protonated DCM is only moderately shifted with respect to that of neutral DCM. Thus far there is no striking difference in the calculated between DANS and DCM that might explain the differences in the absorption spectra of their protonated forms. However, in the case of DCM, while in the neutral the absorption peaks show a pattern similar to DANS, that is, S_1 with significantly higher oscillator strength than S_2-S_5, in protonated DCM there is a "diffusion" of the transition probability from S_1 (mostly) to the S_2 and S_3 higher states, in all solvents considered. For example, the calculated (B3LYP) maxima and oscillator strengths in ethanol for neutral DCM are S_1 (493 nm, 1.38), S_2 (364 nm, 0.20), and S_3 (350 nm, 0.15), whereas in protonated DCM they are S_1 (418 nm, 0.67), S_2 (341 nm, 0.81), and S_3 (307 nm, 0.32). A drawing of the UV−vis spectra of DANS, DCM, and their protonated forms, based on the calculated transition energies and oscillator strengths of the lowest five excited singlet states, as produced by Gaussian 09, is given in Figure 5, where the differences in the absorption spectra between DANS, protonated DANS, DCM, and that of protonated DCM are clearly shown. These results are consistent with the experimental picture (Figure 1b), where the absorption spectrum of protonated DCM does not show a distinct maximum but it absorbs over a rather wide range of wavelengths, with significant overlap with the polymer emission.

Conclusion

Electronic structure calculations have been carried out on the ground and excited electronic states of DANS, DCM, and their protonated forms in order to rationalize the observed differences between the spectra of DANS and DCM upon protonation. It was found that the lowest excited state of DANS, as indicated by the electron density plots of the frontier orbitals, is characterized by a transfer of electronic charge from the dimethylamino group toward the nitrostilbene, which is more pronounced at the twisted secondary minimum energy geometry of the excited state. For neutral DCM the situation is similar to neutral DANS, with the lowest excited state involving transfer of electron density from the dimethylamino group, at both the ground and the excited state equilibrium geometries. For this system, the calculations did not find a twisted excited state minimum. The calculated absorption maxima are in good agreement with the experimental for neutral DANS when the calculations employ the CAM-B3LYP functional, whereas for DCM the B3LYP results are in good agreement with experiment. Emission maxima for DANS in different solvents were only obtained with CAM-B3LYP, whereas for DCM, where available, the B3LYP values for the emission maxima are in better agreement with experimental data.

Upon protonation of DANS, there is no significant charge-transfer contribution to the character of the excited state, S_1, either at the ground state equilibrium geometry or at the S_1 equilibrium geometry. However, the calculations on protonated DCM show that the excited state is characterized by a transfer of charge from the pyran ring toward the rest of the molecule, in both the ground and the excited state equilibrium geometries. In terms of calculated absorption λ_{max}, protonation of DANS results in significant blue shifts, whereas in DCM the blue shifts are smaller, depending on the solvent. Furthermore, the present results show in protonated DCM a "dispersion" of the absorption probability from the lowest excited state to the next two higher states, resulting in absorption over a wide range of wavelengths. Protonated DANS does not show this dispersion but instead a distinct maximum of the oscillator strength is calculated corresponding to absorption into S_1, a characteristic that makes DANS more attractive for absorbance and emission tuning.

The theoretical work presented here is in the direction of understanding the influence of the environment on the structural and spectroscopic characteristics of organic dyes attractive for use in OLEDs technology, sensing, and related applications.

Acknowledgment. I.D.P. and G.T. acknowledge financial support from the EU FP7, Capacities Program, NANOHOST project (GA 201729) and from the NATO grant No. SPS/CBP.MD.CLG.983711.

References and Notes

(1) (a) Rijkenberg, R. A.; Bebelaar, D.; Buma, W. J.; Hofstraat, J. W. *J. Phys. Chem. A* **2002**, *106*, 2446. (b) Cha, M.; Torruellas, W. E.; Stegeman, G. I.; Horsthius, W. H. G.; Möhlmann, G.; Meth, R. J. *Appl. Phys. Lett.* **1994**, *65*, 2648. (c) Beljonne, D.; Bredas, J. L.; Cha, M.; Torruellas, W. E.; Stegeman, G. I.; Hofstraat, J. W.; Horsthius, W. H. G.; Möhlmann, G. R. *J. Chem. Phys.* **1995**, *103*, 7834.

(2) Moran, A. M.; Bartholomew, G. P.; Bazan, G. C.; Myers Kelley, A. *J. Phys. Chem. A* **2002**, *106*, 4928.

(3) Gomez, I.; Reguero, M.; Boggio-Pasqua, M.; Robb, M. A. *J. Am. Chem. Soc.* **2005**, *127*, 7119.

(4) Farztdinov, V. M.; Ernsting, N. P. *Chem. Phys.* **2002**, *277*, 257.

(5) (a) Görner, H. *J. Photochem. Photobiol. A: Chem.* **1987**, *40*, 325. (b) Gruen, H.; Görner, H. *J. Phys. Chem.* **1989**, *93*, 7144.

(6) Maciejewski, A.; Naskrecki, R.; Lorene, M.; Ziolek, M.; Karolczak, J.; Kubicki, J.; Matysiak, M.; Szymanski, M. *J. Mol. Struct.* **2000**, *555*, 1.

(7) Pomogaev, V. A.; Svetlichnyi, V. A.; Pomogaev, A. V.; Svetlichnaya, N. N.; Kopylova, T. N. *High Energy Chem.* **2005**, *39*, 403.

(8) Xu, X.; Zhang, R.; Cao, Z.; Zhang, Q. *J. Theor. Comput. Chem.* **2008**, *7*, 719.

(9) (a) Oberlé, J.; Abraham, E.; Jonusauskas, G.; Rullière, C. *J. Raman Spectrosc.* **2000**, *31*, 311. (b) Oberlé, J.; Abraham, E.; Jonusauskas, G.; Lapouyade, R.; Rullière, C. *Bull. Chem. Soc. Jpn.* **2002**, *75*, 1041.

(10) Jager, W. F.; Sarker, A. M.; Neckers, D. C. *Macromolecules* **1999**, *32*, 8791.

(11) Das, G. P.; Dudis, D. S. *Chem. Phys. Lett.* **1999**, *312*, 57.

(12) Morley, J. O. *J. Phys. Chem.* **1994**, *98*, 13182.

(13) Van Tassle, A. J.; Prantil, M. A.; Fleming, G. R. *J. Phys. Chem. B* **2006**, *110*, 18989.

(14) Marguet, S.; Mialocq, J. C.; Millie, P.; Berthier, G.; Momicchioli, F. *Chem. Phys.* **1992**, *160*, 265.

(15) (a) Suzuki, H.; Hoshino, S. *J. Appl. Phys.* **1996**, *79*, 8816. (b) B.-J. Jung, B.-J.; Yoon, C.-B.; Shim, H.-K.; Do, L.-M.; Zyung, T. *Adv. Funct. Mater.* **2001**, *11*, 430.

(16) Tang, C. W.; Van Slyke, S. A.; Chen, C. H. *J. Appl. Phys.* **1989**, *65*, 3610.

(17) Vasilopoulou, M.; Georgiadou, D. G.; Pistolis, G.; Argitis, P. *Adv. Funct. Mater.* **2007**, *17*, 3477.

(18) Georgiadou, D. G.; Vasilopoulou, M.; Pistolis, G.; Palilis, L. C.; Dimotikali, D.; Argitis, P. *Phys. Stat. Sol. A* **2008**, *205*, 2526.

(19) (a) Li, J.; Liu, D.; Hong, Z.; Tong, S.; Wang, P.; Ma, C.; Lengyel, O.; Lee, C.-S.; Kwong, H.-L.; Lee, S. *Chem. Mater.* **2003**, *15*, 1486. (b) Kann, S.; Liu, X.; Shen, F.; Zhang, J.; Ma, Y.; Zhang, G.; Wang, Y.; Shen, J. *Adv. Funct. Mater.* **2003**, *13*, 603.

(20) (a) Vasilopoulou, M.; Georgiadou, D. G.; Palilis, L. C.; Botsialas, A.; Petrou, P. S.; Kakabakos, S. E.; Argitis, P. *Microelectron. Eng.* **2009**, *86*, 1511. (b) Kim, J.-M. *Macromol. Rapid Commun.* **2007**, *28*, 1191. (c) Vekselman, A. M.; Zhang, C.; Darling, G. D. *Chem. Mater.* **1997**, *9*, 1942.

(21) Parr, R. G.; Yang, W. *Annu. Rev. Phys. Chem.* **1995**, *46*, 701.

(22) Marques, M. A. L.; Gross, E. K. U. *Annu. Rev. Phys. Chem.* **2004**, *55*, 427.

(23) (a) Christiansen, O.; Koch, H.; Jørgensen, P. *Chem. Phys. Lett.* **1995**, *243*, 409. (b) Hättig, C.; Köhn, A. *J. Chem. Phys.* **2002**, *117*, 6939. (c) Hättig, C.; Weigend, F. *J. Chem. Phys.* **2000**, *113*, 5154. (d) Hättig, C. *J. Chem. Phys.* **2003**, *118*, 7751. (e) Köhn, A.; Hättig, C. *J. Chem. Phys.* **2003**, *119*, 5021.

(24) (a) Dreuw, A.; Head-Gordon, M. *Chem. Rev.* **2005**, *105*, 4009. (b) Tamar Stein, T.; Kronik, L.; Baer, R. *J. Am. Chem. Soc.* **2009**, *131*, 2818.

(25) Petsalakis, I. D.; Kerkines, I. S. K.; Lathiotakis, N. N.; Theodorakopoulos, G. *Chem. Phys. Lett.* **2009**, *474*, 278.

(26) Becke, A. D. *J. Chem. Phys.* **1993**, *98*, 1372. (b) Lee, C.; Yang, W.; Parr, R. G. *Phys. Rev. B.* **1988**, *37*, 785.

(27) Schäfer, A.; Huber, C.; Ahlrichs, R. *J. Chem. Phys.* **1994**, *100*, 5829.

(28) Frisch, M. J.; Trucks, G. W.; Schlegel, H. B.; Scuseria, G. E.; Robb, M. A.; Cheeseman, J. R.; Montgomery, J. A., Jr.; Vreven, T.; Kudin, K. N.; Burant, J. C.; Millam, J. M.; Iyengar, S. S.; Tomasi, J.; Barone, V.; Mennucci, B.; Cossi, M.; Scalmani, G.; Rega, N.; Petersson, G. A.; Nakatsuji, H.; Hada, M.; Ehara, M.; Toyota, K.; Fukuda, R.; Hasegawa, J.; Ishida, M.; Nakajima, T.; Honda, Y.; Kitao, O.; Nakai, H.; Klene, M.; Li, X.; Knox, J. E.; Hratchian, H. P.; Cross, J. B.; Adamo, C.; Jaramillo, J.; Gomperts, R.; Stratmann, R. E.; Yazyev, O.; Austin, A. J.; Cammi, R.; Pomelli, C.; Ochterski, J. W.; Ayala, P. Y.; Morokuma, K.; Voth, G. A.; Salvador, P.; Dannenberg, J. J.; Zakrzewski, V. G.; Dapprich, S.; Daniels, A. D.; Strain, M. C.; Farkas, O.; Malick, D. K.; Rabuck, A. D.; Raghavachari, K.; Foresman, J. B.; Ortiz, J. V.; Cui, Q.; Baboul, A. G.; Clifford, S.; Cioslowski, J.; Stefanov, B. B.; Liu, G.; Liashenko, A.; Piskorz, P.; Komaromi, I.; Martin, R. L.; Fox, D. J.; Keith, T.; Al-Laham, M. A.; Peng, C. Y.; Nanayakkara, A.; Challacombe, M.; Gill, P. M. W.; Johnson, B.; Chen, W.; Wong, M. W.; Gonzalez, C.; Pople, J. A. *Gaussian 03, Revision C.02, and Gaussian 09, Revision A. 1.*; Gaussian, Inc.: Wallingford CT, 200.

(29) Peach, M. J. G.; Benfield, P.; Helgaker, T.; Tozer, D. J. *J. Chem. Phys.* **2008**, *128*, 044118.

(30) Cozi, M.; Scalmani, G.; Rega, N.; Barone, V. *J. Chem. Phys.* **2002**, *117*, 43.

(31) Pedone, A.; Bloino, J.; Monti, S.; Prampolini, G.; Barone, V. *Phys. Chem. Chem. Phys.* **2010**, *12*, 1000.

(32) (a) Ahlrichs, R.; Bär, M.; Häser, M.; Horn, H.; Kölmel, C. *Chem. Phys. Lett.* **1989**, *162*, 165. (b) *TURBOMOLE, version 5.10*; http://www.turbomole.com.

(33) Förster, T. *Disc. Faraday Soc.* **1959**, *27*, 7.

JP100338D